

# A new model for deflagration fronts in reactive fluids

M. Reinecke<sup>1</sup>, W. Hillebrandt<sup>1</sup>, J.C. Niemeyer<sup>2</sup>, R. Klein<sup>3</sup>, and A. Gröbl<sup>1</sup>

<sup>1</sup> Max-Planck-Institut für Astrophysik, Karl-Schwarzschild-Strasse 1, D-85740 Garching, Germany

<sup>2</sup> LASR, Enrico Fermi Institute, University of Chicago, Chicago, IL 60637, USA

<sup>3</sup> Konrad-Zuse-Zentrum für Informationstechnik Berlin, Takustrasse 7, D-14195 Berlin-Dahlem, Germany

Received 20 November 1998 / Accepted 19 April 1999

**Abstract.** We present a new way of modeling deflagration fronts in reactive fluids, the main emphasis being on turbulent thermonuclear deflagration fronts in white dwarfs undergoing a Type Ia supernova explosion. Our approach is based on a level set method which treats the front as a mathematical discontinuity and allows full coupling between the front geometry and the flow field (Smiljanovski et al., 1997). With only minor modifications, this method can also be applied to describe contact discontinuities. Two different implementations are described and their physically correct behaviour for simple testcases is shown. First results of the method applied to the concrete problems of Type Ia supernovae and chemical hydrogen combustion are briefly discussed; a more extensive analysis of our astrophysical simulations is given in Reinecke et al. (1998).

**Key words:** hydrodynamics – nuclear reactions, nucleosynthesis, abundances – turbulence – methods: numerical – stars: supernovae: general

## 1. Introduction

Numerical simulations of turbulent combustion have always been a challenge, mainly because of the large range of length scales involved. In astrophysics, prominent examples are Type Ia supernovae, where the length scales of relevant physical processes range from  $10^{-4}$  cm to several  $10^8$  cm. In the currently favoured scenario the explosion starts as a deflagration in the flamelet regime near the center of the star. At the corresponding densities, the typical width of the conductive flame is less than 1 mm (Timmes & Woosley, 1992). Rayleigh-Taylor unstable blobs of hot burnt material are thought to form which rise and lead to shear-induced turbulence at their interface with the unburnt gas. This turbulence increases the effective surface area of the flamelets and thereby the rate of fuel consumption over its laminar value; the hope is that finally a fast deflagration might result, in agreement with phenomenological models of Type Ia explosions (Nomoto et al., 1984).

A multidimensional direct numerical simulation of such an event is – and will always be – computationally infeasible; there-

fore, small scale effects like turbulence, diffusion and heat conduction need to be incorporated in form of phenomenological models. Despite considerable progress in the field of modeling turbulent combustion for astrophysical flows (see, e.g., Niemeyer 1995), the correct numerical representation of the thermonuclear deflagration front is still a weakness of Type Ia simulations; this is mainly due to the fact that in those simulations the conductive flame is not properly resolved, but must be made several orders of magnitude thicker than in reality. The artificially increased width of the reaction zone is a prerequisite for the reactive-diffusive flame model (Khokhlov, 1993), which has been used by most authors so far. In this approach the burning region is stretched out over several grid zones to ensure an isotropic flame propagation speed. Typical values for the numerical flame width range from 4–5 (Khokhlov, 1993) to 8–10 grid cells (Niemeyer, 1994). However, the artificially soft transition from fuel to ashes stabilizes the front against hydrodynamical instabilities on small length scales, which in turn results in an underestimation of the flame surface area and – consequently – of the total energy generation rate.

The front tracking method described in this paper is based on the so-called *level set technique* that has been in use for several years in the engineering sciences. It was introduced by Osher & Sethian (1988) who used the zero level set of a  $n$ -dimensional scalar function to represent  $(n - 1)$ -dimensional front geometries. Sussman et al. (1994) give equations for the time evolution of such a level set which is passively advected by a flow field; this approach can be used to track contact discontinuities, for example. Smiljanovski et al. (1997) extend this method to allow the tracking of fronts additionally propagating normal to themselves, e.g. deflagrations and detonations. In contrast to the artificial broadening of the flame in the reaction-diffusion-approach, their algorithm is able to treat the front as an exact hydrodynamical discontinuity. Considering the fact that the real width of the conductive flame in a Type Ia supernova is several orders of magnitude smaller than the typical grid cell sizes in multidimensional simulations, this is a very good approximation.

The outline of this paper is as follows: In Sect. 2 we present the main ideas and governing equations of our approach. Two different implementations of the flame model are described in detail in Sect. 3. Sect. 4 is dedicated to the results of simple

---

Send offprint requests to: M. Reinecke  
(martin@mpa-garching.mpg.de)

testcases, whereas Sect. 5 lists some results of the application of our numerical scheme to “real world” problems. Finally, we give a summary of open issues and an outlook on future work in Sect. 6.

## 2. The level set method

The central aspect of our front tracking method is the association of the front geometry (a time-dependent set of points  $\Gamma$ ) with an isoline of a so-called level set function  $G$ :

$$\Gamma := \{\mathbf{r} \mid G(\mathbf{r}) = 0\} \quad (1)$$

Since  $G$  is not completely determined by this equation, we can additionally postulate that  $G$  be negative in the unburnt and positive in the burnt regions, and that  $G$  be a “smooth” function, which is convenient from a numerical point of view. This smoothness can be achieved, for example, by the additional constraint that

$$|\nabla G| \equiv 1 \quad (2)$$

in the whole computational domain, with the exception of possible extrema and kinks of  $G$ . The ensemble of these conditions produces a  $G$  which is a signed distance function, i.e. the absolute value of  $G$  at any point equals the minimal front distance.

The normal vector to the front is defined as

$$\mathbf{n} := -\frac{\nabla G}{|\nabla G|} \quad (3)$$

and thus points towards the unburnt material.

The task is now to find an equation for the temporal evolution of  $G$  such that the zero level set of  $G$  behaves exactly as the flame. Such an expression can be obtained by the consideration that the total velocity of the front consists of two independent contributions: it is advected by the fluid motions at a speed  $\mathbf{v}$  and it propagates normal to itself with a burning speed  $s$ .

Since for deflagration waves a velocity jump usually occurs between the pre-front and post-front states, we must explicitly specify which state  $\mathbf{v}$  and  $s$  refer to; traditionally, the values for the unburnt state are chosen. Therefore, one obtains for the total front motion

$$\mathbf{D}_f = \mathbf{v}_u + s_u \mathbf{n}. \quad (4)$$

The total temporal derivative of  $G$  at a point  $\mathbf{P}$  attached to the front must vanish, since  $G$  is, by definition, always 0 at the front:

$$\frac{dG_{\mathbf{P}}}{dt} = \frac{\partial G}{\partial t} + \nabla G \cdot \dot{\mathbf{x}}_{\mathbf{P}} = \frac{\partial G}{\partial t} + \mathbf{D}_f \cdot \nabla G = 0 \quad (5)$$

This leads to the desired differential equation describing the time evolution of  $G$ :

$$\frac{\partial G}{\partial t} = -\mathbf{D}_f \cdot \nabla G \quad (6)$$

This equation, however, cannot be applied on the whole computational domain: Firstly,  $\mathbf{D}_f$  has a physical meaning in the immediate vicinity of the front only and may be undefined elsewhere. Secondly, using this equation everywhere will in

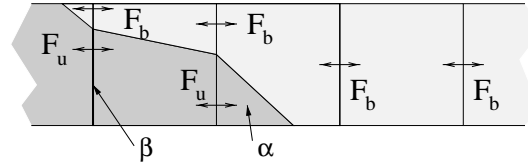


**Fig. 1.** Illustration of the basic principles of the level set method according to Smiljanovski et al. (1997): The piecewise linear front cuts the mixed cells into burnt and unburnt parts.  $\alpha$  is the unburnt volume fraction of a cell,  $\beta$  is the unburnt area fraction of a cell interface. The fluxes  $F_u$  and  $F_b$  are calculated from the reconstructed states.

most cases destroy  $G$ 's distance function property (Eq. 2). As a consequence, this might lead to the buildup of very steep slopes in  $G$  which are likely to cause numerical problems (Sussman et al., 1994). Therefore additional measures must be taken in the regions away from the front to ensure a “well-behaved”  $|\nabla G|$  (for implementation details, see Sect. 3.1.2).

The situation is further complicated by the fact that the quantities  $\mathbf{v}_u$  and  $s_u$  which are needed to determine  $\mathbf{D}_f$  are not readily available in the cells cut by the front. In a finite volume context, these cells contain a mixture of pre- and post-front states instead. Nevertheless one can assume that the conserved quantities (mass, momentum and total energy) of the mixed state satisfy the following conditions:

$$\bar{\rho} = \alpha \rho_u + (1 - \alpha) \rho_b \quad (7)$$

$$\bar{\rho} \bar{\mathbf{v}} = \alpha \rho_u \mathbf{v}_u + (1 - \alpha) \rho_b \mathbf{v}_b \quad (8)$$

$$\bar{\rho} \bar{e} = \alpha \rho_u e_u + (1 - \alpha) \rho_b e_b \quad (9)$$

Here  $\alpha$  denotes the volume fraction of the cell occupied by the unburnt state. In order to reconstruct the states before and behind the flame, a nonlinear system consisting of the equations above, the Rankine-Hugoniot jump conditions and a burning rate law must be solved. The technical details are described in Sect. 3.2.2.

Having obtained the reconstructed pre- and post-front states in the mixed cells, it is not only possible to determine  $\mathbf{D}_f$ , but also to separately calculate the fluxes of burnt and unburnt material over the cell interfaces. Consequently, the total flux over an interface can be expressed as a linear combination of burnt and unburnt fluxes weighted by the unburnt interface area fraction  $\beta$ :

$$\bar{\mathbf{F}} = \beta \mathbf{F}_u + (1 - \beta) \mathbf{F}_b \quad (10)$$

(see Fig. 1).

## 3. Implementation

In this section we concentrate on the case of a deflagration wave, but the modifications needed to model contact discontinuities are straightforward: for this case, the front propagation speed ( $s$  or  $s_u$ ) and the formation enthalpy ( $q$ ) have to be zero in all following equations, which leads to an overall simplification of the numerical scheme.

For our calculations, the front tracking algorithm was implemented as an additional module for the hydrodynamics code PROMETHEUS (Fryxell et al., 1989). Two independent and completely different implementations were realized:

- In the simpler approach, the  $G$ -function plays a somehow passive role: It is advected by the fluid motions and by burning and is only used to determine the source terms for the reactive Euler equations. We will refer to this algorithm as *passive implementation*. It must be noted that there exists no *real* discontinuity between fuel and ashes in this case; the transition is smeared out over about three grid cells by the hydrodynamical scheme, and the level set only indicates where the thin flame front *should* be. However, the numerical flame is still considerably thinner than in the reaction-diffusion approach.
- The second implementation (called *complete implementation*) contains in-cell-reconstruction and flux-splitting as proposed by Smiljanovski et al. (1997); therefore it should exactly describe the coupling between the flame and the hydrodynamic flow.

### 3.1. Passive implementation

#### 3.1.1. $G$ -transport

Since the front motion consists of two distinct contributions, it is appropriate to use an operator splitting approach for the time evolution of  $G$ . The advection term due to the fluid velocity  $\mathbf{v}_F$  can be written as

$$\frac{\partial G}{\partial t} = -\mathbf{v}_F \nabla G, \quad (11)$$

or in conservative form

$$\int_V \frac{\partial(\rho G)}{\partial t} d^3r + \oint_{\partial V} -\mathbf{v}_F \rho G d\mathbf{f} = 0 \quad (12)$$

(Mulder et al., 1992). This equation is identical to the advection equation of a passive scalar, like the concentration of an inert chemical species. Consequently, this contribution to the front propagation can be calculated by PROMETHEUS itself without requiring complicated modifications. As a consequence, the discrete values of the level set function have to be stored at the centers of the grid cells, like the hydrodynamical variables  $\rho$ ,  $T$ , etc.

The additional flame propagation due to burning is calculated at the end of each time step according to the following procedure:

First the four discrete spatial derivatives of  $G$  are obtained in each cell:

$$D_{x,ij}^+ := \frac{G_{i+1,j} - G_{i,j}}{x_{i+1} - x_i} \quad D_{x,ij}^- := \frac{G_{i,j} - G_{i-1,j}}{x_i - x_{i-1}} \quad (13)$$

$$D_{y,ij}^+ := \frac{G_{i,j+1} - G_{i,j}}{y_{j+1} - y_j} \quad D_{y,ij}^- := \frac{G_{i,j} - G_{i,j-1}}{y_j - y_{j-1}} \quad (14)$$

At the boundaries of the computational domain some of the above equations cannot be applied (e.g.  $D_{x,1j}^-$ ). In these cases, the gradient is set to 0 for reflecting boundaries and extrapolated in zeroeth order for outflow boundaries.

Afterwards, the relevant derivatives are determined by simple upwinding with respect to the propagation direction of the front:

$$D_{x,ij} = \begin{cases} D_{x,ij}^+ & \text{for } D_{x,ij}^+ > 0 \quad \text{and } D_{x,ij}^- > 0 \\ D_{x,ij}^- & \text{for } D_{x,ij}^+ < 0 \quad \text{and } D_{x,ij}^- < 0 \\ \bar{D}_{x,ij} & \text{for } (D_{x,ij}^- \cdot D_{x,ij}^+) \leq 0 \end{cases} \quad (15)$$

where  $\bar{D}_{x,ij} := 0.5(|D_{x,ij}^-| + |D_{x,ij}^+|)$ .

The new  $G$ -value is then defined by

$$G'_{ij} = G_{ij} + \Delta t s_{ij} \sqrt{D_{x,ij}^2 + D_{y,ij}^2}. \quad (16)$$

#### 3.1.2. Re-initialization

As was mentioned in Sect. 2, an additional correction step has to be applied in the regions away from the front in order to keep  $G$  a signed distance function. This task can be accomplished in several ways. Sussman et al. (1994), for example, suggest a pseudo-time approach, where the equation

$$\frac{\partial G}{\partial \tau} = \frac{G}{|G| + \varepsilon} (1 - |\nabla G|) \quad (17)$$

is solved iteratively until convergence is obtained. Here,  $\varepsilon$  denotes an empirical quantity with a value comparable to the length of a grid cell. While being quite efficient, this method has the drawback that it changes *all*  $G$ -values, even those near the front; consequently, the front might be moved by small amounts during the re-initialization (Sethian, 1996).

This potential problem is avoided by the following algorithm which we used for our simulations:

- The coordinates of all zero crossings of  $G$  between neighbouring grid points are calculated by linear interpolation; if, e.g.,  $G_{i,j} > 0$  and  $G_{i+1,j} < 0$ , the zero crossing is at

$$x_z = x_i + \left| \frac{G_{i,j}}{G_{i+1,j} - G_{i,j}} \right| (x_{i+1} - x_i) \quad (18)$$

and

$$y_z = y_j \quad (19)$$

The ensemble of all points  $(x_z, y_z)$  is a discrete representation of the zero level set.

- For all grid points, the minimum distance to one of the points  $(x_z, y_z)$  is determined:

$$d_{ij} = \min_n \sqrt{(x_i - x_{z,n})^2 + (y_j - y_{z,n})^2} \quad (20)$$

- The corrected value for  $G_{ij}$  is a weighted average of the original value and  $d_{ij}$ , such that

$$G'_{ij} := H(d_{ij})G_{ij} + (1 - H(d_{ij}))\text{sgn}(G_{ij})d_{ij}. \quad (21)$$

$H$  denotes a function, which is essentially 1 for small arguments and smoothly drops to 0 near a given threshold. In this work, we used the expression

$$H(d) = \left( 1 - \tanh \frac{d - d_0}{\delta/3} \right) / \left( 1 - \tanh \frac{-d_0}{\delta/3} \right). \quad (22)$$

For this equation, the transition takes place in a region of the width  $\delta$  around  $d_0$ . Satisfying results have been obtained for  $d_0 \approx 3\Delta$  and  $\delta \approx \Delta$ , where  $\Delta$  represents the width of a grid cell.

The weighting with  $H(d)$  has the effect that values near the flame are practically left unchanged, while the values farther away represent a distance function in good approximation.

### 3.1.3. Source terms

After the update of the level set function in each time step, the change of chemical composition and total energy due to burning is calculated in the cells cut by the front. In order to obtain these values, the volume fraction  $\alpha$  occupied by the unburnt material is determined in those cells by the following approach: from the value  $G_{ij}$  and the two steepest gradients of  $G$  towards the front in  $x$ - and  $y$ -direction a first-order approximation  $\tilde{G}$  of the level set function is calculated; then the area fraction of cell  $ij$  where  $\tilde{G} < 0$  can be found easily. Based on these results, the new concentrations of fuel, ashes and energy are obtained:

$$X'_{\text{Ashes}} = \max(1 - \alpha, X_{\text{Ashes}}) \quad (23)$$

$$X'_{\text{Fuel}} = 1 - X'_{\text{Ashes}} \quad (24)$$

$$e'_{\text{tot}} = e_{\text{tot}} + q(X'_{\text{Ashes}} - X_{\text{Ashes}}) \quad (25)$$

In principle this means that all fuel found behind the front is converted to ashes and the appropriate amount of energy is released. The maximum operator in Eq. (23) ensures that no “reverse burning” (i.e. conversion from ashes to fuel) takes place in the cases where the average ash concentration is higher than the burnt volume fraction; such a situation can occur in a few rare cases because of unavoidable discretization errors of the numerical scheme.

## 3.2. Complete implementation

In this approach the discrete values of  $G$  are defined on the cell corners instead of the cell centers, because this simplifies the calculation of the geometrical quantities  $\alpha$  and  $\beta$ , which are needed for the reconstruction and flux-splitting steps. In the following sections all quantities defined on cell corners are described by fractional indices: e.g.  $G_{i+1/2,j+1/2}$  denotes the  $G$  value in the top right corner of cell  $ij$ .

### 3.2.1. Geometrical quantities

The knowledge of the front normal  $\mathbf{n}$  and the unburnt volume fraction  $\alpha$  in the mixed cells is a prerequisite for the reconstruction of burnt and unburnt hydrodynamical states. The normal is derived from the discrete gradient

$$\left(\frac{\partial G}{\partial x}\right)_{ij} = \frac{1}{2} \left( \frac{G_{i+1/2,j+1/2} - G_{i-1/2,j+1/2}}{x_{i+1/2} - x_{i-1/2}} + \frac{G_{i+1/2,j-1/2} - G_{i-1/2,j-1/2}}{x_{i+1/2} - x_{i-1/2}} \right) \quad (26)$$

$$\left(\frac{\partial G}{\partial y}\right)_{ij} = \frac{1}{2} \left( \frac{G_{i+1/2,j+1/2} - G_{i+1/2,j-1/2}}{y_{j+1/2} - y_{j-1/2}} + \frac{G_{i-1/2,j+1/2} - G_{i-1/2,j-1/2}}{y_{j+1/2} - y_{j-1/2}} \right). \quad (27)$$

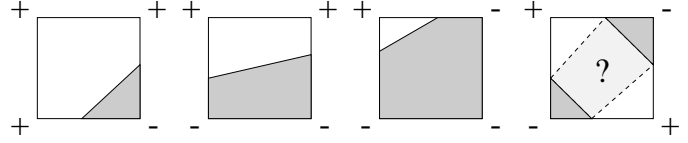


**Fig. 2.** Determination of  $\alpha$  in a mixed cell. The signs on the cell corners denote the sign of the  $G$  function. The rightmost sketch shows a situation where two different geometrical interpretations are possible and  $\alpha$  is not uniquely defined.

According to Eq. (3),  $\mathbf{n}_{ij}$  is then given by

$$\mathbf{n}_{ij} = -\frac{(\nabla G)_{ij}}{|(\nabla G)_{ij}|}. \quad (28)$$

The value for  $\alpha$  is found by determining the zeros of  $G$  on all cell edges, connecting them with straight lines and calculating the surface area behind this approximated flame. Fig. 2 shows all topologically different situations. While calculating  $\alpha$  in the first three cases is trivial, the fourth case is ambiguous since two different front geometries are possible; for this situation, we set  $\alpha$  to the mean value of the two possibilities. Fortunately, such a geometrical constellation is quite rare in hydrodynamical simulations.

### 3.2.2. Reconstruction

In order to obtain the hydrodynamical state vectors  $\mathbf{U}_u$  and  $\mathbf{U}_b$  from the average  $\bar{\mathbf{U}}$  in the mixed cells, a nonlinear equation system has to be solved. The first three equations have already been presented in Sect. 2 (Eqs. 7–9). It is convenient to split the velocity vector into a normal and a tangential part with respect to the front; Eq. (8) then reads

$$\bar{\rho}\bar{v}_n = \alpha\rho_u v_{n,u} + (1 - \alpha)\rho_b v_{n,b} \quad (29)$$

and

$$v_{t,u} = v_{t,b} = \bar{v}_t. \quad (30)$$

Further, the reconstructed states must satisfy the Rayleigh criterion and the Hugoniot jump condition for the internal energy:

$$(\rho_u s_u)^2 = -\frac{p_b - p_u}{V_b - V_u} \quad (31)$$

$$e_{i,b} - e_{i,u} = q - \frac{(p_b + p_u)}{2}(V_b - V_u) \quad (32)$$

Here,  $e_i$  is defined as  $e_{\text{tot}} - v^2/2$  and  $V := 1/\rho$ . The pressures are given by the equation of state:

$$p_u = p_{\text{EOS}}(\rho_u, e_{i,u}, \mathbf{X}_u) \quad (33)$$

and

$$p_b = p_{\text{EOS}}(\rho_b, e_{i,b}, \mathbf{X}_b) \quad (34)$$

Additionally, the jump condition for the normal velocity component reads

$$v_{n,b} - v_{n,u} = s_u \left(1 - \frac{\rho_u}{\rho_b}\right). \quad (35)$$

To complete the system, a burning rate law is required. Usually this will be the equation for the laminar burning speed, depending on the unburnt state variables. In our case of highly turbulent burning in the flamelet regime, the flame speed can be derived from the turbulent kinetic sub-grid energy  $e_{sg}$  (Niemeyer & Hillebrandt, 1995a,b):

$$s_u = \sqrt{2e_{sg}} \quad (36)$$

The ensemble of all the equations above can be solved with any of standard iterative method. Our implementation uses a globally converging Broyden solver (Broyden, 1965; Press et al., 1992). In contrast to the popular Newton-Raphson approach, this algorithm converges even for relatively bad initial guesses, which is important for our application.

### 3.2.3. Transport

The algorithms presented in the three following subsections are designed for use with a *directional splitting* scheme and are thus orientation independent. Therefore we will only describe the numerical procedure for the  $x$ -sweeps.

For the complete implementation a simple, non-conservative approach is used to obtain the  $G$ -values at the new time level:

$$G^{n+1} = G^n - \Delta t D_x^n \frac{\partial G^n}{\partial x} \quad (37)$$

Several complications arise from the fact that values for  $D_x$ , which is defined in the center of the mixed cells, are needed at the cell corners. Since  $D$  only has a physical meaning in the mixed cells, its value in all other cells may be chosen arbitrarily. It can be shown analytically that the distance function property of  $G$  is preserved if the condition

$$\mathbf{n} \nabla (D \mathbf{n}) = 0 \quad (38)$$

is satisfied, i.e. if the flame propagation velocity is constant along the “field lines” of  $G$ . Consequently, the values for  $D$  in the whole computational domain are obtained by spreading out the values in the mixed cells in the direction of  $\mathbf{n}$  and  $-\mathbf{n}$ .

In the next step,  $D_x$  in the middle of the cell interfaces is calculated by simple averaging

$$D_{x,i,j+1/2} = \frac{1}{2}(D_{x,i,j} + D_{x,i,j+1}), \quad (39)$$

and the corner values  $D_{x,i+1/2,j+1/2}$  are determined by upwinding. Depending on the sign of  $D_x$  at the corner, the appropriate discrete derivative of  $G$  is chosen; if  $D_x$  is negative, one takes  $(\partial G / \partial x)$  at the right side, and vice versa. Now all quantities needed in Eq. (37) are known.

Because of the discrete nature of the grid, it is in most cases impossible to satisfy condition (38) exactly; therefore a re-initialization step is required for the complete implementation also. This is done in exactly the same fashion as described in Sect. 3.1.2.

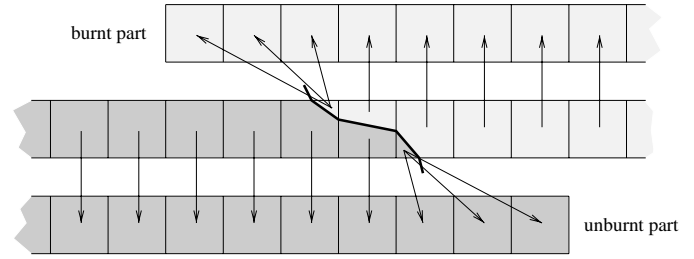


**Fig. 3.** Splitting of a state vector containing burnt and unburnt cells into partial vectors with only fuel or ashes. The necessary ghost cells at the artificial boundaries are calculated by zeroeth order extrapolation.

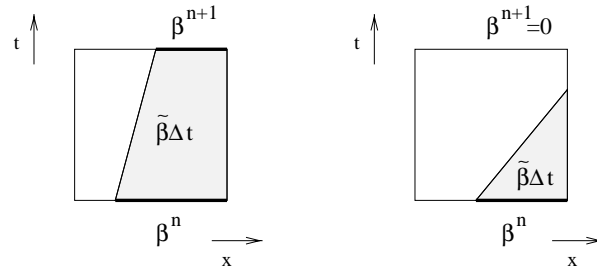


**Fig. 4.** Determination of the average unburnt interface area fraction  $\tilde{\beta}$  for two different cases. As can be seen, simply taking the average of old and new time level does not always produce the correct result.

### 3.2.4. Flux-splitting

In order to compute the total fluxes across a mixed cell interface, it is necessary to solve the Riemann problems for burnt and unburnt states separately. To achieve this, each grid vector is split into a sequence of completely burnt and unburnt partial vectors. During this process, artificial boundaries are created at the front location for which boundary conditions must be specified. Following Smiljanovski et al. (1997), this is done by zeroeth order extrapolation of the cells at the boundary (see Fig. 3 for illustration). The PPM algorithm implemented in PROMETHEUS is then used to calculate the hydrodynamical fluxes for the partial vectors.

Now Eq. (10) is applied to compose the total fluxes. However, it is in many cases insufficient to use the unburnt interface fraction  $\beta$  at the beginning of the time step in this formula, especially when the flame enters or leaves a cell during the time step. Therefore we calculate the average of  $\beta$  over the time step (see also Fig. 4):

$$\tilde{\beta} = \frac{1}{\Delta t} \int_{t^n}^{t^{n+1}} \beta dt \quad (40)$$

The composed flux then reads

$$\tilde{\mathbf{F}} = \tilde{\beta} \mathbf{F}_u + (1 - \tilde{\beta}) \mathbf{F}_b. \quad (41)$$

### 3.2.5. Source terms

The amount of matter consumed by the flame in a mixed cell during a time step is given by

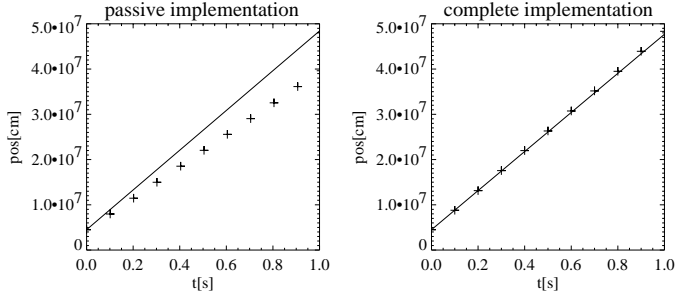


**Fig. 5.** Time dependent position of a planar flame propagating in positive  $x$ -direction for both implementations of the front tracking algorithm. The lines indicate the theoretically predicted behaviour.

$$\Delta m = \int_{t^n}^{t^{n+1}} A s_u \rho_u dt, \quad (42)$$

where  $A$  denotes the flame surface in this cell. For the  $x$ -sweep in a directional splitting scheme one obtains

$$\Delta m_x = \int_{t^n}^{t^{n+1}} n_x^2 A s_u \rho_u dt. \quad (43)$$

The factor  $n_x^2$  is introduced by the projection of the flame on the  $y$ -axis (or on the  $yz$ -plane in three dimensions) and by the projection of the burning speed on the  $x$ -axis. In the  $i$ -th cell, the ratio of the projected flame surface and the surface of a cell interface is approximately given by  $|\tilde{\beta}_{i+1/2} - \tilde{\beta}_{i-1/2}|$ . Thus one obtains for the source terms

$$\Delta X_{\text{Ashes},i} = \frac{\Delta t}{\Delta x_i} \frac{\rho_{u,i}}{\bar{\rho}_i} \left| s_{u,i} n_{x,i} (\tilde{\beta}_{i+1/2} - \tilde{\beta}_{i-1/2}) \right| \quad (44)$$

$$\Delta X_{\text{Fuel},i} = -\Delta X_{\text{Ashes},i} \quad (45)$$

$$\Delta e_{\text{tot},i} = q \Delta X_{\text{Ashes},i}. \quad (46)$$

#### 4. Numerical tests

A set of testcases was run with both of the implementations presented above to determine the ability of the numerical schemes to represent thermonuclear flames. Our main criteria were the reproduction of a given burning velocity and the isotropy of the front propagation. Additionally, we investigated the behaviour of the algorithms for complex situations, like the merging of two flame kernels and cusp formation in a sinusoidally perturbed flame.

At  $t = 0$ , the thermodynamical state of the unburnt matter was characterized by  $\rho_u = 5 \cdot 10^8 \text{ g/cm}^3$ ,  $T_u = 5 \cdot 10^8 \text{ K}$ , and  $X_{12C,u} = X_{16O,u} = 0.5$ . The energy release for the fusion to  $^{56}\text{Ni}$  is  $q = 7 \cdot 10^{17} \text{ erg/g}$ , and the burning speed  $s_u$  was set to  $3 \cdot 10^7 \text{ cm/s}$ .

For all tests we used a cartesian grid with a cell size of  $1.5 \cdot 10^6 \text{ cm}$ .

##### 4.1. 1D flames

In a first test we investigated a planar flame propagating in positive  $x$ -direction with reflecting boundaries at the left, top and bottom edges of the computational domain and an outflow

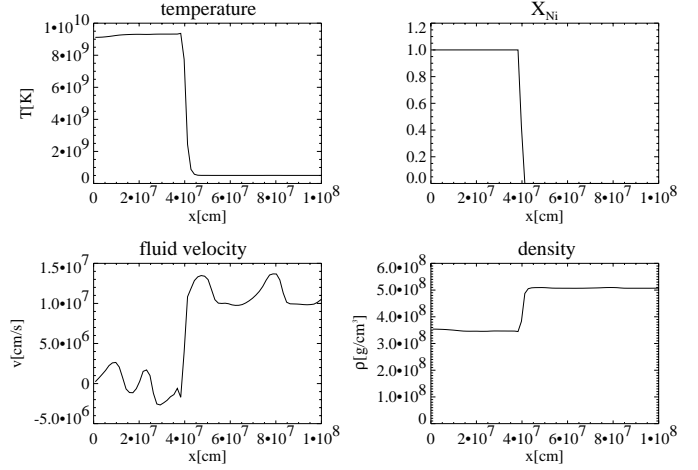


**Fig. 6.** Planar flame propagation test: Temperature, nickel concentration, fluid velocity and density at  $t = 1\text{s}$  for the passive implementation.

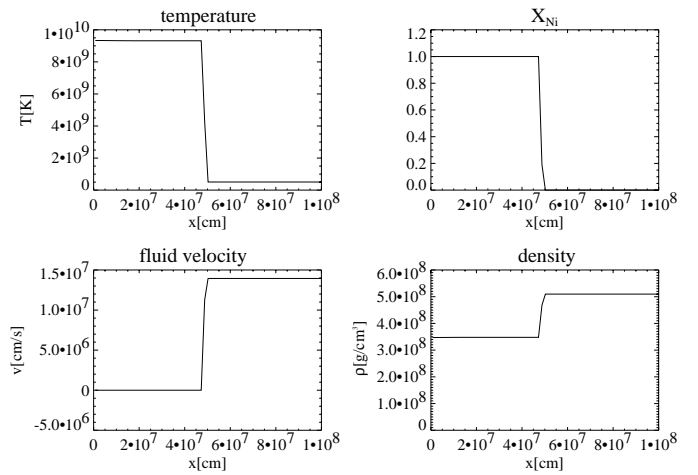


**Fig. 7.** Planar flame propagation test: Temperature, nickel concentration, fluid velocity and density at  $t = 1\text{s}$  for the complete implementation.

boundary to the right. The grid consisted of  $128 \times 4$  cells. Under these circumstances the material behind the front should be at rest and the absolute front velocity with respect to the grid is expected to be

$$s_b := s_u \rho_u / \rho_b, \quad (47)$$

which corresponds to about  $4.4 \cdot 10^7 \text{ cm/s}$  for our initial conditions.

As can be seen in Fig. 5, the agreement of simulation and predictions is excellent for the complete implementation, whereas the passive implementation underestimates the flame velocity by about 20%. Figs. 6 and 7 show the profiles of temperature, nickel concentration, velocity and density for both algorithms at  $t = 1\text{s}$ . Again, the complete implementation gives exactly the expected results: two constant states that are separated by a mixed cell. With the exception of the fluid velocity, the picture is nearly the same for the passive implementation; here the transition is smeared out over about three grid cells by PPM. The velocity profile shows strong oscillations in this case; one

also notes that the average fluid motion in the unburnt material is noticeably slower than for the complete implementation.

All the deviations in the passive approach can be explained by the fact that the flame is not advected with the speed of the unburnt matter as postulated in Eq. (4), but by the *average* speed in the burning cells. Depending on whether the flame just entered the cell or is about to leave it, this quantity is closer to the unburnt resp. the burnt velocity but never reaches the desired  $v_u$ . As a consequence, the flame propagates too slowly and at a non-uniform speed, thereby causing fluctuations in the velocity field.

To further investigate this behaviour of the passive implementation, two additional tests with  $\rho_u = 3 \cdot 10^9 \text{g/cm}^3$  and  $\rho_u = 5 \cdot 10^7 \text{g/cm}^3$  were performed. In these cases the flame propagation speed was underestimated by 14% and 28%, respectively. Since the error grows roughly proportionally with the density jump, these observations support our interpretation.

However, for the special case of turbulent burning in the interior of white dwarfs, these seemingly large errors can be tolerated: firstly, the velocity jump across the flame is quite small compared to the burning velocity; secondly, our model for the turbulent burning speed is based on dimensional analysis and therefore  $s_u$  itself could carry an uncertainty much larger than the 28% mentioned above.

A first order correction for the underestimation of the burning speed in the passive implementation can be done in a quite straightforward way for this concrete physical problem and will be incorporated in future versions of the code.

## 4.2. 2D flames

### 4.2.1. One circular flame

To test the isotropy of both algorithms, the propagation of an initially circular flame was simulated on a grid of  $50 \times 50$  cells with outflow boundaries; some snapshots of the front geometry are shown in Fig. 8. While deviations from the circle shape do occur, they are sufficiently small for both implementations. The difference in the flame propagation speed is still present and nearly of the same size as in the one-dimensional simulation.

### 4.2.2. Two merging circular flames

On the same grid as in the simulation above, the merging of two circular flame kernels was investigated to demonstrate the ability of the level set approach to handle topological changes. As the results indicate, the formation of a single front happens smoothly and without numerical difficulties (see Fig. 9). The slight deformation of the fronts before the merging can be explained by the interaction of the velocity fields generated by both flames.

### 4.2.3. Perturbed planar flame

Fig. 10 shows the temporal evolution of a sinusoidally perturbed flame propagating in positive  $x$ -direction. As expected, the trail-

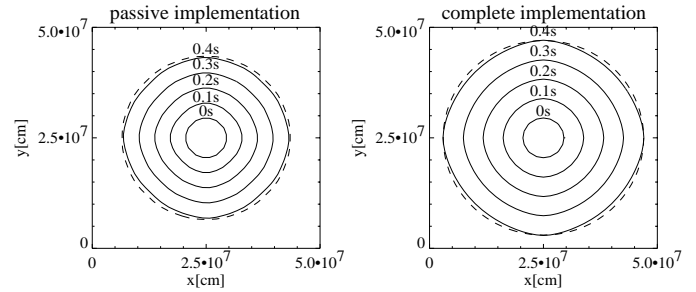


**Fig. 8.** Snapshots of the front geometry for circular flame propagating outwards. The dashed lines represent exact circles and have been added to allow easier judgement of the flame geometry.

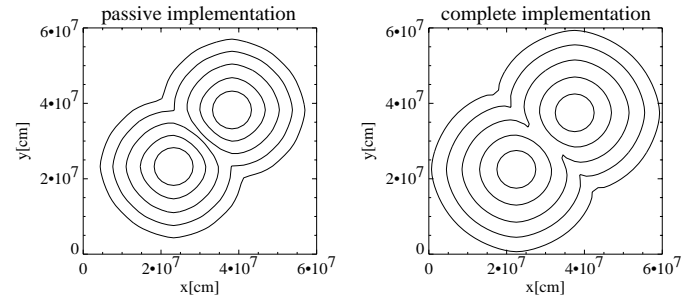


**Fig. 9.** Evolution of the front geometry for two merging circular flames. The time difference between subsequent snapshots is 0.1s (from inside to outside).

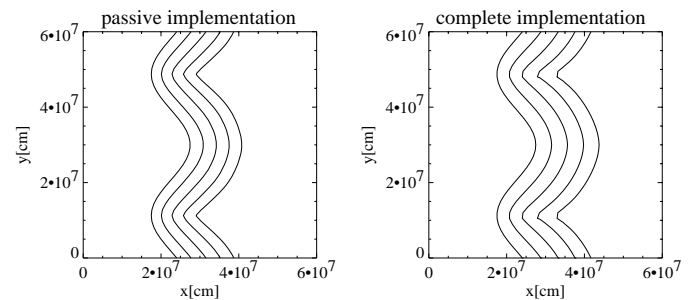


**Fig. 10.** Evolution of the front geometry for a sinusoidally perturbed flame. The time difference between subsequent snapshots is 0.1s (from left to right).

ing part of the front becomes narrower until a cusp is formed; afterwards, the flame geometry remains practically unchanged. The short vertical section of the flame that can be seen in the right panel of Fig. 10 is an artifact of the rather poor resolution: since the (expected) cusps are located exactly at the  $y$ -position of the cell centers and the level set is stored at the cell corners, they cannot be seen in this discretization.

## 4.3. Sensitivity of the reconstruction equations

The results of all tests described above show that both implementations of the level set method can be used to model turbulent thermonuclear combustion in Type Ia supernovae. Since the complete version is more accurate, it would be the method

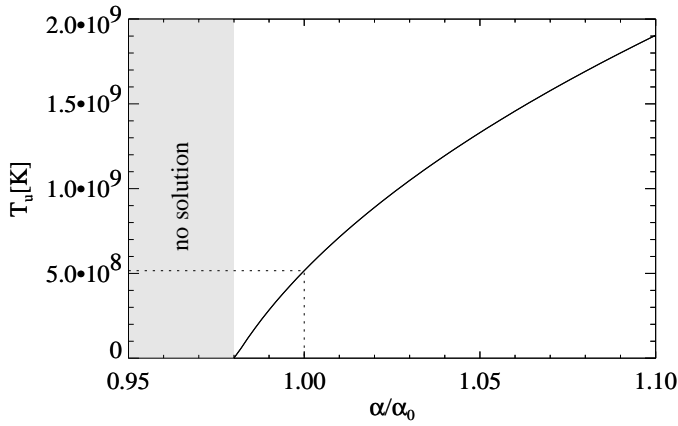


**Fig. 11.** Reconstructed temperature of the unburnt material for varying deviations in  $\alpha$ . Below  $\alpha/\alpha_0 < 0.98$ , the reconstruction fails.

of choice. Unfortunately, however, it has turned out that the straightforward implementation of the reconstruction as described above leads to numerical difficulties when applied to the “real” situation in a white dwarf including density and pressure gradients and gravitational forces. In our supernova simulations with the complete implementation, after a few time steps the reconstruction in many mixed cells failed because the internal energy of the unburnt state reached values for which the equation of state is undefined:

$$e_{i,u} < e_{\text{EOS}}(\rho_u, T = 0\text{K}, X_{\text{fuel}}) \quad (48)$$

Discretization errors in the input values are the most likely reason for this divergence. To test the reaction of the reconstruction algorithm on such uncertainties, the following experiment was performed:

From a given pre- and post-front state that exactly fulfill the Rankine-Hugoniot jump conditions a mixed state is synthesized according to Eqs. (7)-(9) for an  $\alpha_0$  equal to 0.5. Then a reconstruction is tried for this mixed state, but for a slightly different  $\alpha$  (i.e. for an  $\alpha$  with some uncertainty). In Fig. 11, the reconstructed temperature of the unburnt material is plotted against the introduced error in  $\alpha$ . It can be easily seen that for  $\alpha/\alpha_0 < 0.98$  a reconstruction of pre- and post-front states becomes impossible. For highly curved fronts, as they are expected in Type Ia supernovae, the deviations of  $\alpha$  from the exact value can become much higher than that, because  $\alpha$  is obtained for a piecewise linear approximation of the front. At first glance, one would expect an improvement if the front geometry was modeled with higher accuracy, e.g. by approximation with quadrics. But in this case, other problems appear: the number of different topological configurations in a cell explodes, and, most importantly, there is no way to define the normal  $\mathbf{n}$  that is required by the reconstruction equations.

Because of these numerical problems, we have not yet been able to simulate Type Ia supernovae with the complete implementation of the front tracking scheme. An investigation of the properties of the reconstruction equations and, if possible, creation of a more robust system is subject of future work. However, introducing just an artificial viscosity to limit the curvature of

the flame front may be an easy way to stabilize the numerical scheme.

## 5. Applications

### 5.1. Type Ia supernovae

The passive implementation of the level set method has been used to model the turbulent flame front in the early stages of Type Ia supernova explosions. To allow direct comparison with the reaction-diffusion model, our initial conditions were chosen as similar as possible to the simulations done by Niemeyer & Hillebrandt (1995b). Our results show a flame which is perturbed due to Rayleigh-Taylor- and Kelvin-Helmholtz-instabilities on all scales down to a few grid cells (see Fig. 12). An extensive discussion of this simulation as well as simulations with other initial conditions can be found in Reinecke et al. (1998).

### 5.2. Chemical hydrogen combustion

The complete implementation has already been successfully used to model turbulent flame fronts in lean hydrogen-air mixtures. Fig. 13 shows the merging of three flame parts in a mixture of 15% hydrogen in air in a box with an outflow boundary to the right and reflecting boundaries elsewhere. Since small disturbances are amplified by material diffusion in the case of hydrogen flames, the burning speed was modified depending on the curvature of the front.

## 6. Conclusions

We have presented a numerical model to describe deflagration fronts with a reaction zone much thinner than the cells of the computational grid. In contrast to the currently favoured method for astrophysical simulations (Khokhlov, 1993), our approach provides a considerably sharper transition from fuel to ashes, thereby allowing the growth of hydrodynamical instabilities on smaller scales and generally the evolution of small features in the flame.

Two different implementations of the model have been developed and tested; for simple initial conditions, both versions produce results acceptable for our needs. However, because of the mentioned numerical problems the complete implementation cannot be employed for supernova simulations without modification.

In addition to modeling flames, the level set method described in this paper can also be used for tracking contact discontinuities with only minor modifications; therefore, any application in astrophysical hydrodynamics dealing with one of these phenomena might benefit from this numerical scheme.

*Acknowledgements.* This work was supported in part by the Deutsche Forschungsgemeinschaft under Grant Hi 534/3-1 and by DOE under contract No. B341495 at the University of Chicago. The computations were performed at the Rechenzentrum Garching on a Cray J90. The authors thank E. Bravo for many constructive suggestions which led to a significant improvement of this paper.



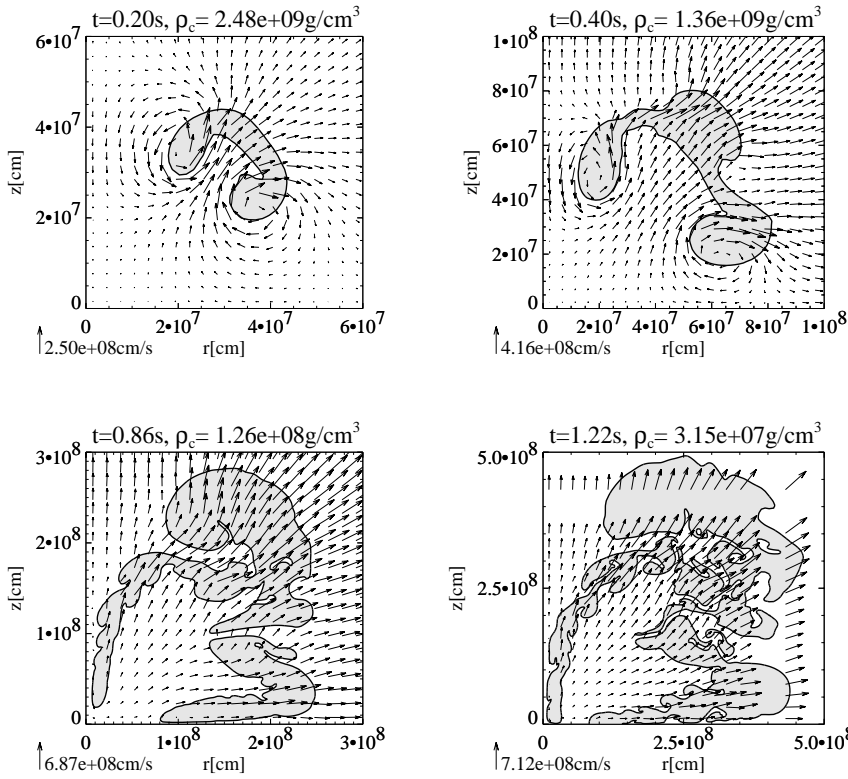


**Fig. 12.** Temporal evolution of front geometry and velocity field after igniting a single, circular bubble near the center of the white dwarf. Note that the scales change from snapshot to snapshot.

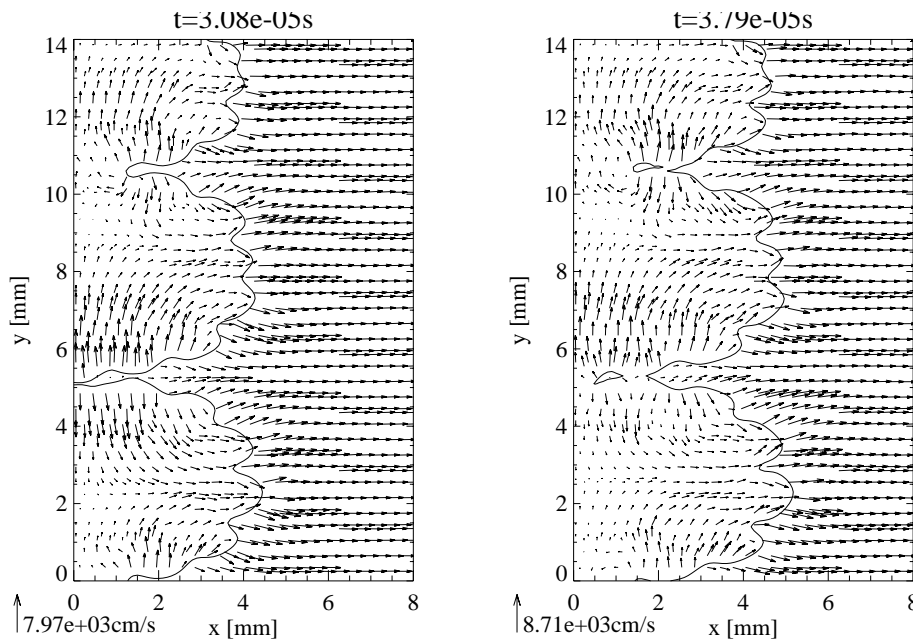


**Fig. 13.** Chemical combustion in a lean hydrogen-air mixture on a grid consisting of  $100 \times 140$  cells, with reflecting borders at the left, top and bottom and a flowout boundary at the right. Due to the high material diffusion of hydrogen, little disturbances are amplified. This was modeled by using a curvature-dependent flame speed.

## References

- Broyden C.G., 1965, *Mathematics of Computation* 19, 577  
 Fryxell B.A., Müller E., Arnett W.D., 1989, MPA Preprint 449  
 Khokhlov A.M., 1993, *ApJ* 419, L77  
 Mulder W., Osher S., Sethian J.A., 1992, *JCP* 100, 209  
 Niemeyer J.C., 1994, *Turbulente thermonukleare Brennfronten in Weißen Zwergen*. Master's Thesis, Max-Planck-Institut für Astrophysik, Garching  
 Niemeyer J.C., 1995, *On the Propagation of Thermonuclear Flames in Type Ia Supernovae*. Ph.D. Thesis, Max-Planck-Institut für Astrophysik, Garching  
 Niemeyer J.C., Hillebrandt W., 1995a, *ApJ* 452, 769  
 Niemeyer J.C., Hillebrandt W., 1995b, *ApJ* 452, 779  
 Nomoto K., Thielemann F.K., Yokoi K., 1984, *ApJ* 286, 644  
 Osher S., Sethian J.A., 1988, *JCP* 79, 12  
 Press W.H., Teukolsky S.A., Vetterling W.T., Flannery B.P., 1992, *Numerical Recipes in C*. Cambridge University Press, Cambridge

- Reinecke M.A., Hillebrandt W., Niemeyer J.C., 1999, *A&A* 347, 731
- Sethian J.A., 1996, *Level Set Methods*. Cambridge University Press, Cambridge
- Smiljanovski V., Moser V., Klein R., 1997, *Comb. Theory and Modeling* 1, 183
- Sussman M., Smereka P., Osher S., 1994, *JCP* 114, 146
- Timmes F.X., Woosley S.E., 1992, *ApJ* 396, 649